frontiers | Frontiers in Physics

TYPE Review
PUBLISHED 29 September 2022
DOI 10.3389/fphy.2022.1015603

Check for updates

OPEN ACCESS

EDITED BY
John Goree,
The University of Iowa, United States

REVIEWED BY
Neeraj Chaubey,
The University of Iowa, United States
Mehran Shahmansouri,
Arak University, Iran
Job Beckers,
Eindhoven University of Technology, Netherlands

*CORRESPONDENCE
Lénaïc Couëdel,
lenaic.couedel@usask.ca,
lenaic.couedel@univ-amu.fr

SPECIALTY SECTION
This article was submitted to Low-Temperature Plasma Physics, a section of the journal Frontiers in Physics

RECEIVED 09 August 2022
ACCEPTED 02 September 2022
PUBLISHED 29 September 2022

CITATION
Couëdel L (2022), Temporal dusty plasma afterglow: A review. *Front. Phys.* 10:1015603. doi: 10.3389/fphy.2022.1015603

COPYRIGHT
© 2022 Couëdel. This is an open-access article distributed under the terms of the Creative Commons Attribution License (CC BY). The use, distribution or reproduction in other forums is permitted, provided the original author(s) and the copyright owner(s) are credited and that the original publication in this journal is cited, in accordance with accepted academic practice. No use, distribution or reproduction is permitted which does not comply with these terms.

Temporal dusty plasma afterglow: A review

Lénaïc Couëdel[1,2]*

[1]Physics and Engineering Physics Department, University of Saskatchewan, Saskatoon, SK, Canada, [2]CNRS, Aix-Marseille Univerité, Laboratoire PIIM, UMR 7345, Marseille, France

In complex plasmas, dust particles are charged through their interactions with the electrons and ions of the surrounding plasma. In low-temperature laboratory plasmas, dust particles most commonly acquire a negative charge. In particular, in a laboratory glow-discharge plasma, the typical charge for a micrometer-size grain generally attains a few thousands of electronic charges. Under stable discharge conditions, this large negative charge is relatively well-characterized. However, for unsteady discharge conditions, the charge can differ and even fluctuate. In particular, when the power source of the discharge is turned off, the charged species of the plasma diffuse away and recombine into neutral species: this is a temporal afterglow. When dust particles are present inside a temporal plasma afterglow, the diffusion of charged species and the plasma decay dynamics are affected. Moreover, the dust particle charges also evolve during the afterglow period. In the late afterglow, dust particles are known to keep residual charges. The value of these residual charges strongly depends on the ambipolar-to-free diffusion transition. In addition, the presence of a constant electric field, causing ions to drift through the neutral gas, has a strong influence on the final dust particle residual charges, eventually leading to large positive residual charges. In this review article, the dynamics of temporal complex plasma afterglow are discussed. Experimental and theoretical results are presented. The basics of temporal afterglow modeling are also given.

KEYWORDS

plasma, afterglow, dust, charge, ambipolar, diffusion

1 Introduction

Complex (dusty) plasmas are partially ionized gases containing charged solid nano- or micro-grains (or dust). In laboratory experiments, dust particles can be either injected or grown directly in the plasma. The grain charge develops mainly due to the collections of the ambient electrons and ions, which, under steady-state conditions, balance each other. In laboratory low-temperature plasmas, the grains are usually negatively charged due to the higher mobility of the plasma electrons [1–6]. Depending on the conditions, other processes can also significantly influence dust charges. For example, positively charged particles are sometimes observed due to photoemission induced by ultraviolet radiation [7–9]. Thermionic or secondary emission of electrons can also lead to positive dust charges, as is the case in fusion plasmas [10–12].

In laboratory experiments, injected dust particles are usually micron-size particles. Due to their mass, injected particles are usually confined near the electrode where the electric force can balance the gravity force unless the experiment is performed under microgravity [13–15] or a thermophoresis force is applied [16,17] to create a dust cloud filling the bulk plasma. Dense clouds of submicron particles light enough to stay in the bulk plasma can be obtained using reactive gases such as silane [18–20] and acetylene [21–23] or using a target sputtered with ions coming from the plasma [24–26]. In complex plasmas, the electric charge of the grains is obviously a key parameter. Indeed, it determines the interactions of the dust particles with the background ions and electrons and the grain–grain interactions [such as in complex plasma crystals [27,28]]. It is also fundamental in many processes, such as the ion drag force [29,30] and electric charge shielding [31]. Knowledge of the charge is, therefore, essential to the understanding of the basic properties of a complex plasma, the dust dynamics, and developing methods for grain manipulations [32]. In plasma discharges in which particles are growing, the nanoparticle charges have a fundamental role during the agglomeration stage [33,34]. While the charge of dust particles in steady-state homogeneous plasma has been extensively studied and is relatively well-known (see Chapter 2 of Melzer et al. [6] and references therein), dust particle charging in unsteady plasma conditions is still poorly understood. This is, for example, the case for dust charging in an afterglow plasma.

An afterglow plasma is a mixture of ions, electrons, excited species, and neutral gas that occurs when the plasma is not actively powered and ionization cannot be sustained ("stationary" or "temporal" afterglow, where time is the main parameter) or far enough from an active discharge region in flowing gas ("flowing" or "spatial" afterglow, where space is the main parameter) [35]. In an afterglow plasma, the energy deposited in the discharge to ionize the gas and excite metastable species relaxes slowly. In particular, the cooling of electrons is due to collisional and diffusion processes [36–41]. The time evolution of the electron density and the electron temperature is very sensitive to the discharge chamber geometry and the discharge conditions [41]. In the afterglow, the plasma species are continuously lost by diffusion. While in the early stage of the afterglow, quasi-neutrality holds, and the charge species transport obeys ambipolar diffusion, in the later stage, quasi-neutrality is no longer obeyed, and ambipolar diffusion fails at describing charge species transport [42–45]).

When dust particles are present in the plasma, the evolution of the plasma afterglow are modified due to the influence of dust on ion and electron diffusion and energy losses [46–50]. In addition, dust dynamics in an afterglow plasma is modified with respect to their motion in a steady-state plasma or in neutral gas. Due to the influence of dust on plasma decay and the existence of dust residual charges in the late afterglow [51], these effects can be particularly important in dusty pulsed discharges in which a significant amount of time corresponds to afterglow plasma [52,53]. While dusty spatial (or flowing) afterglow is a field of active research [54–56,56–60], this review article is restricted to temporal (or stationary) dusty plasma afterglows. The article is structured as follows. In Section 2, a review of the different experimental and theoretical results is given. The results are divided into two categories: the influence of dust particles on plasma decay during the afterglow (Section 2.1) and dust dynamics and dust residual charges in plasma afterglow (Section 2.2). In Section 3, the basics of the modeling of the time evolution of a temporal dusty plasma afterglow are discussed. Finally, in Section 4, a summary of the main results is given.

2 Dusty plasma afterglow: main results

2.1 Influence of dust on plasma decay

Dimoff and Smy [46], for the first time, reported on the influence of dust particles on the decay of a temporal plasma afterglow. By injecting microparticle (radius $r_d = 15\ \mu$m) in the afterglow of pulsed linear argon discharge at a pressure $p = 1.9$ Torr, Dimoff and Smy [46] showed that due to absorption-recombination on the microparticle surfaces, the plasma decay time is drastically reduced compared to dust-free discharges. Under their experimental conditions, they were able to enhance the natural decay of the plasma by a factor of ~ 50 (for a microparticle number density $n_d \sim 10^4\ \mathrm{cm}^{-3}$). The decay enhancement was correctly attributed to the flux of positive ions on the negatively charged particles, but the effect of the relatively large microparticle number density on the particle charge was not taken into account, leading to an overestimation of the microparticle absorption frequency τ_Q^{-1}. The results were re-analyzed by Couëdel et al. [61]. Taking into account the microparticle charge decrease at large dust number density, it was shown that τ_Q^{-1} does not increase linearly with dust density. More details about the plasma decay process are given in Section 3.

The effect of dust particles on the evolution of a pulse discharge is also significant. For example, in a pulsed argon acetylene discharge, depending on experimental conditions, the electron density time evolution can exhibit anomalous behaviour. When nanoparticles are grown during the plasma-on phase, the electron density decreases when the rf-power is turned on, while it increases when the rf-power is switched off [52]. This anomalous electron density increase occurred between 250 μs and 500 μs in the power-off phase, depending on the discharge conditions and the dust particle size. This counterintuitive observation was attributed to the charging/decharging of nanoparticles [52]. Stefanovic et al. [62] reported that secondary electron emission due to electron impact could not explain the release of electrons in the early afterglow due to the

too low value of the intrinsic secondary electron yield from carbonaceous dust material. Several different other mechanisms were proposed to explain the electron release in the early afterglow: ion impact, UV-photons, collision with metastable atoms and fast neutral atoms, thermionic emission, or field emission. Note that this reported behaviour is similar to observations in pulsed discharge containing negative ions. For example, in a pulsed inductively-coupled radio-frequency plasma in oxygen (pressure range from 0.5 to 200 Pa), a peak of the electron density is also observed in the early afterglow (maximum effect for pressures around 50 Pa) [63]. The density peak is due to the loss of the balance between electron attachment and detachment processes. When the discharge power is switched off, rapid cooling of the electrons occurs, inhibiting the production of new negative ions, while the existing negative ions are destroyed by collisions which lead to the release of free electrons in the early afterglow. Additional experiments performed in a pulsed capacitively-coupled radio-frequency (cc-rf) Ar/C_2H_2 discharge have shown that the presence of dust particles increases the argon metastable atom density by an order of magnitude due to the increase of electron temperature after dust formation [64]. However, in the considered experimental conditions (p = 10 Pa and rf power 10 W < P_W < 80 W), the main loss mechanism for metastable atoms is diffusion to the electrodes and not quenching at the surface of the dust particles. Denysenko et al. [65] developed zero-dimensional, space-averaged global models to simulate dust-free and dusty argon plasma afterglow. They suggested that the electron density increase observed in the early afterglow [52] could be due to metastable pooling, but metastable–dust interactions might also contribute.

Schweigert and Alexandrov [66] and Alexandrov et al. [67] performed particle-in-cell (PIC) Monte Carlo collision (MCC) simulations to study the influence of nanoparticles on an argon plasma afterglow under conditions similar to the experiments by Berndt et al. [52]. Using the simulated ion and electron energy distribution functions (IEDF and EEDF, respectively), Schweigert and Alexandrov [66] and Alexandrov et al. [67] have shown that the loss of fast electrons to the electrode in the early afterglow (diffusion cooling) leads to a change of the electron and ion currents on the dust particle surfaces and a drop of the dust floating potential. Alexandrov et al. [67] reported that the main production of desorbed electrons occurs during this electron cooling phase (30–50 μs into the afterglow). The resulting release of electrons by the dust particles might explain the experimentally observed anomalous electron density growth, but the simulated anomalous electron density growth time is an order of magnitude shorter than the one measured by Berndt et al. [52]. Schweigert and Alexandrov [66] and Alexandrov et al. [67] also included metastable argon atoms in their simulations. They showed that, in the afterglow, metastable–metastable ionization maintains a higher electron density and higher electron energy (a second peak centered at 7.3 eV becomes visible on the EEDF). However, the resulting electrons do not directly contribute to the observed anomalous electron density increase but enhance the effect of dust decharging on the anomalous electron density increase.

Sikimić et al. [68,69] performed experimental studies on plasma afterglow with large dust density under conditions very similar to those in the experiments by Berndt et al. [52]. They showed that the negative self-bias voltage that remains on the powered electrode during the afterglow (the self-bias voltage decays exponentially as in an RC circuit) is sufficiently large to induce secondary electrons by collisions between the positive ions and the electrode. Using a time-dependant zero-dimensional, space-averaged global model taking into account thermal electrons with Maxwellian EEDF, energetic electrons generated by metastable-metastable collisions (metastable pooling), and secondary electrons generated by ion collisions with the bias electrodes, Denysenko et al. [70] were able to estimate the effect of the secondary electron emission on the afterglow electron density as a function of the secondary emission yield. They reported that the effect of secondary electrons is not as large as metastable pooling in the dusty plasma afterglow, while in the dust-free afterglow, their effect might surpass metastable pooling. In addition, the thermal electron density increase due to secondary electron emission is about a few percent in both dusty and dust-free plasma afterglows. However, while the simulation results of Denysenko et al. [70] are in good qualitative agreement with experimental measurements, there is a quantitative discrepancy, especially in the late afterglow. It was suggested that this discrepancy might be due to a deviation of the EEDF from a Maxwellian distribution. In particular, the tail of the EEDF in the late afterglow may be depleted due to diffusion cooling of the high-energy electrons toward chamber walls and the dust particles [39]. The influence of non-Maxwellian EEDF on the evolution of plasma afterglow was further investigated by Denysenko et al. [71–73]. Their studies revealed that electron absorption plays an important role in determining the electron energy probability function (EEPF) in a dusty afterglow [71]: using a kinetic description of the EEPF and solving the electron Boltzmann equation using the method of characteristics, EEPF analytical expressions were obtained for different initial EEPFs exhibiting a tail at energies larger than the dust floating potential (including Maxwellian and Druyvesteyn EEPFs). Denysenko et al. [71] showed that the presence of dust particles affects particle absorption and plasma conductivity and significantly reduces the number of energetic electrons with respect to the dust-free case. In the study by Denysenko et al. [73], using a spatially averaged global model taking into account metastable atoms, the influences of the EEPF shape on reaction rates, of the pulsed frequency ν_p and of the duty cycle on pulsed discharge properties were investigated in both dust-free (pure Ar discharge) and dusty (Ar/C_2H_2 mixture) scenarios. It was shown that a Druyvesteyn EEPF matches better experimental

results. They also showed that ν_p has a strong impact on the metastable atom density but with different effects in the dust-free and dusty cases: in dust-free plasma, high pulsing frequency results in higher metastable densities than in a continuous discharge; on the contrary, when the discharge contains dust, the metastable atom density is smaller at high pulsing frequency. The difference might be explained by a faster change of the effective electron temperature in dusty afterglow due to collection of energetic electrons by the dust particles. Denysenko et al. [73] also showed that in the late afterglow, non-Maxwellian EEPF results in smaller electron density due to an enhanced electron flux to the wall, while in the dusty case, it results in an increase of the electron density due to electron collisions with metastable atoms and other molecules remaining from the dust-formation stage.

Pulsed dusty Ar/C_2H_2 were also simulated in detail using a zero-dimensional, space-averaged global model by taking into account the chemical processes of Ar/C2H2 plasma. Both the glow and the afterglow were investigated. The glow results were compared to mass spectroscopy measurements. Furthermore, Denysenko et al. [72] found that the presence of dust particles plays a major role in determining the properties of the discharge (in the glow and afterglow phases). The collection of electrons and ions by the dust particles results in an increase in the effective electron temperature, the ion density and the metastable density with respect to dust-free discharge while decreasing the density of acetylene molecules and hydrocarbon ions. Finally, it was shown that the anomalous peak in the electron density during the afterglow could be due to an enhancement of electron production due to the larger density of metastable atoms that ionize acetylene molecules by collision.

2.2 Dust dynamics, dust decharging, and residual charges in plasma afterglow

The first hints at the existence of dust residual charges in temporal plasma afterglow were obtained by Barkan and Merlino [74]. They electrostatically trapped a microparticle cloud (a dust "ball") in the high-potential region of an anode double layer formed in a single-ended Q-machine plasma. When the confining electric fields were removed, a radial "explosion" of the microparticle cloud was reported and explained by Coulomb repulsion. Saxena et al. [75] combined a spatially averaged plasma decay model during the afterglow with molecular dynamics in order to simulate the dust cluster explosion under conditions similar to the experiment by Barkan and Merlino [74]. During the plasma-on phase, the micron/sub-micron–sized particles evolved in a confining potential until a steady-state dust ball was obtained, the confinement was removed rapidly during the afterglow phase, and the dust trajectories were simulated in the time-varying plasma afterglow. Saxena et al. [75] found that the nature of the explosion when the discharge is switched off and the resulting dust acceleration depend critically on the pressure of the background neutral gas. At low gas pressure, it was found that the explosion is due to unshielded Coulomb repulsion between the dust particles and yields maximum acceleration. In the high-pressure regime, the dust ball expansion is explained by (screened) Yukawa repulsive interactions and results in a weaker acceleration in agreement with experimental findings. These two regimes (dust ball explosion and dust ball expansion) were further investigated by Piel and Goree [76] without simulating the time evolution of the background plasma afterglow. However, Saxena et al. [75]'s model of plasma decay only took into account electron-neutral collision for electron cooling and ignored diffusion cooling, which is significant at low pressure [36–41].

Another hint at the existence of residual charges came from the studies by Childs and Gallagher [77] in the afterglow of a dusty plasma (the dust particle density was $n_d \sim 10^7$ cm^{-3}, and the particle radius was $r_d \simeq 6.5$ nm [78]). By recording the light scattered by a dust particle cloud with and without a bias applied to the electrode after the rf power was switched off, the fraction of charged dust particles was measured. They found that about ~50% of the dust particles remained charged in the afterglow. According to their analysis, the final dust particle charge distribution only contained dust particles with charges equal to + 1e, 0e, and − 1e, where e is the elementary charge.

Ivlev et al. [51] reported experiments with the PKE-Nefedov laboratory on board the International Space Station [13] that undoubtedly showed the existence of residual charges on microparticles in the late afterglow of a capacitively coupled radio-frequency discharge (cc-rf). After switching off the rf power, a low-frequency sinusoidal voltage applied to one electrode triggered particle oscillations with amplitudes higher at the periphery of the dust cloud, thus, revealing the microparticle residual electric charges. A simple global model of dusty plasma afterglow, taking into account the loss of electrons and ions by diffusion to the reactor's wall and on dust particles and electron cooling by collision with the neutral atoms, was able to qualitatively explain the results.

Detailed measurements of residual charges were later performed by Couëdel et al. [79]. 200 nm radius particles were grown into a cc-rf argon discharge (see Mikikian et al. [80] for details on particle growth), and an upward thermophoretic force was used to balance the gravitational force. Then, as in Ivlev et al. [51]'s study, a low-frequency voltage was applied to one electrode. It triggered particle oscillations keeping residual charges. Couëdel et al. [79] found that positively-charged, negatively-charged, and neutral dust particles coexisted for a long time after the discharge was switched off with a mean negative residual charge of a few electrons ($|Q_{d_{res}}| \sim 3e - 5e$ depending on pressure). Using Ivlev et al. [51]'s simple decharging model, four stages of the temporal dusty plasma afterglow were identified (and further described by

Couëdel et al. [81–83]) to explain the existence of residual charges. The stages are as follows: stage I, the temperature relaxation stage during which the electrons rapidly cool down, resulting in a fast decrease of the dust particle equilibrium charge; stage II, the plasma density decay stage during which the diffusion of ions and electrons is ambipolar, and the dust charge remains almost constant while starting to deviate from its equilibrium value as the dust charging time becomes gradually larger than the plasma density decay time; stage III, the transition from ambipolar to free diffusion stage which starts when the Debye length becomes comparable to the diffusion length or the Havnes parameter $P_H = Z_d n_d / n_e \sim 1$ (Z_d is the dust particle charge number and n_e is the electron density) during which the dust charge decreases due to an ion current much larger than the electron current because of the faster decrease of the electron density; and stage IV, the frozen stage when the plasma density has become so low that the dust particle charge cannot change anymore. The process is illustrated in Figure 1. In the studies by Couëdel et al. [81–83], using the same experimental set-up as Couëdel et al. [79], dust charge distributions were measured in the late complex plasma afterglow. It was found again that the mean residual charge is negative, but the tail of the distribution extends into the positive-charge region. Numerical simulations taking into account the discreteness of the charging process [84] and taking into account the transition from ambipolar to free diffusion [42–44,85–88] for the evolution of the plasma parameters were performed [82]. The existence of positively charged particles was then explained by the relative broadening of the dust charge distribution in the late stage of the plasma afterglow. The transition from ambipolar to free diffusion plays a major role in the evolution of dust charge distribution. It starts early in the plasma afterglow, as soon as $\Lambda/\lambda_{D_e} \sim 100$, where Λ is the diffusion length and λ_{D_e} is the electron Debye length. The electrons and ions diffuse at different rates, resulting in a smaller mean dust particle charge and broadening of the dust charge distribution. It is of note that Ivlev et al. [51] and Couëdel et al. [81–83]'s models also only took into account electron-neutral collision for the electron temperature decay and ignored diffusion cooling, which is significant at low pressure [36–41].

Dedicated experiments on the spatial distribution of residual charges across a dust cloud trapped in the gap of a cc-rf discharge (the PK-3 Plus laboratory [14]) under microgravity conditions were later performed in the International Space Station [89]. After switching off the power supply, a low-frequency sinusoidal voltage was applied to the electrodes, and the residual charges were deduced from the amplitudes of the resulting particle oscillations. When no additional dc bias was applied to the electrodes ("free decharging" conditions), a symmetric residual charge distribution with a sharp peak centered on zero was observed, but positively and negatively charged particles were homogeneously observed over the cloud. However, a decharging experiment conducted with an additional constant dc bias applied to the electrode (resulting in a dc electric field of

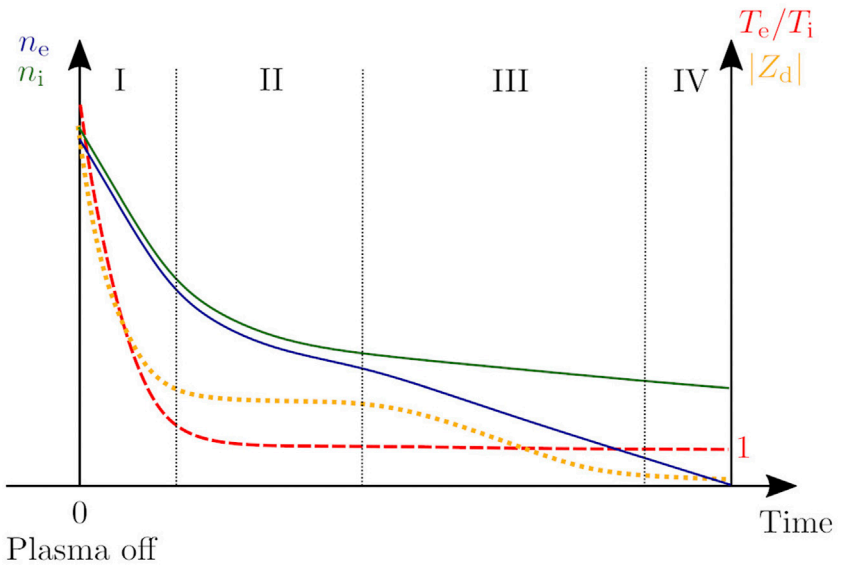

FIGURE 1
(Color on-line) Illustration of the evolution of the plasma parameters and dust charge during the afterglow. The different stages are as follows. Stage I: temperature relaxation; stage II: plasma density decay determined by ambipolar diffusion; stage III: transition to free diffusion; stage IV: frozen stage.

6.67 V/cm in the gap between the electrodes) resulted in most microparticles acquiring a positive residual charge with an asymmetric residual charge distribution centered on + 15e and a significant residual charge gradient along the direction of the applied electric field. Wörner et al. [89] suggested that the drift of charged species induced by the external electric field in the late afterglow and the rapid loss of free electrons were most probably at the origin of the asymmetric charge distribution.

Filatova et al. [90] also studied the process of decay of dust structures formed from polydisperse grains injected into an rf discharge (discharge in air at p = 100 Pa and dust radii $0.1 < r_d < 0.25\ \mu$m). By measuring dust velocities in the plasma afterglow and using the balance of forces acting on the grains, they were able to estimate the dust number density, the dust size, and the dust residual charges. Negative residual charges comprised in the range from − 1e to − 10e, depending on the grain size, were reported.

In his PhD dissertation [91], Schneider reported experimental results in the temporal dusty plasma afterglow of a cc-rf discharge with an argon pressure p = 1–100 Pa and an rf power P_{rf} = 1–10 W. Very large positive residual charges (up to + 5000e) were measured. In his experiment, a dc electric field of the order 10^2 V/cm was applied during the afterglow. The motion of individual microspheres was recorded using video cameras, and, depending on the experimental conditions, the measured residual charges had values varying from negative to positive. Schneider also reported that the rf power, the gas pressure, or the microparticle's position above the electrode did not have a significant influence on the residual charge.

Chaubey et al. [92] also performed an experiment on dust residual charge. In a cc-rf argon discharge at f_{rf} = 13.56 MHz with an argon pressure p = 1.067 Pa, 8.69 μm diameter melamine spherical particles were levitated and formed and two-dimensional plasma crystal. Then, the power was abruptly shut down, and the microparticles fell (note that the particle arrangement was not significantly altered during the fall [93]). In this experiment, due to the large value of the coupling capacitor, the negative self-bias of the powered electrode that develops naturally when the plasma is on ($V_{dc} \simeq -150$ V), decayed in a timescale of ~3 s, a time much longer than the plasma afterglow timescales, therefore, maintaining a large quasi dc electric field between the electrodes during the afterglow period. By studying the trajectories of the dust grains, particle accelerations were extracted, and Chaubey et al. [92] found that the grains fell much faster than expected when gravity alone acts. Using force balance in the afterglow (gravity, neutral drag force, and electric force), they measured very large positive residual charges of the order + 10^4e. They also showed experimentally that the residual charges increased with the reduced electric field E/n_g, where E is the electric field in between the electrode and n_g is the neutral gas number density. The large positive charges were explained by the ion drift through the neutral gas induced by the electric field. Indeed, since a larger value of the reduced electric field E/n_g leads to a larger ion kinetic energy, more positive ions can be collected by a grain and the maximum possible residual positive charge is attained if the grain's surface potential reaches values equal to the ion kinetic energy before all ions have diffused away and the grain's charge freezes.

Residual charges can affect the motion of a dust cloud as a whole in a plasma afterglow. Couëdel et al. [94] studied the motion of an entire dust-particle cloud in the afterglow of a complex plasma. They showed that the dust cloud dynamics were modified by the dust particle residual charges. Meyer and Merlino [95] and Merlino et al. [96] studied the dynamics of dust clouds in an afterglow plasma. They observed a variety of cloud behaviour ranging from simple Coulomb expansion/explosion to Coulomb fission. The observed differences in behaviour seemed to indicate that the dust cloud dynamics and the dust residual charges in the afterglow are very sensitive to the initial dust cloud configuration (shape and dust density) and its position in the discharge. Merlino et al. [97] reported more precisely on the splitting (fission) of a suspension of charged microparticles into two fragments in a plasma afterglow. They proposed that the triggering mechanism for the dust cloud fission could be a pinching instability driven by the ion drag force, but further experimental and theoretical studies are needed to confirm this hypothesis. Finally, Chaudhuri et al. [98] reported on the observation of nonlinear dust pulse structures (particles flowing through each other (uni-directional or counter-streaming)) in afterglow complex plasma under microgravity conditions on board the International Space Station. The dust pulses were triggered when the plasma was switched off in the presence of a low-frequency external electric excitation.

Dust decharging and residual charges were also studied theoretically and numerically. Denysenko et al. [99] studied the decharging of particles using a spatially averaged global model of the plasma afterglow. Using the results from previous PIC-MCC simulations [66], the electron temperature decay time was set at τ_T = 50 μs. The model took into account electron production from ground-state ionization, secondary emission due to ion–dust collision and metastable–dust collision, metastable pooling, and electron losses on plasma walls and dust particles. The time-dependent dust charge in the plasma afterglow was calculated using different approaches: 1) the rate coefficient for the collection of electrons by dust particles was deduced from the electron balance equation using the experimentally measured decays of the electron density $n_e(t)$ and metastable density $n_m(t)$ in the afterglow; 2) the rate coefficient for collection of electrons by dust particles was directly calculated from the Orbital Motion Limited (OML) theory [100] and the contribution from the Maxwellian thermal electron and energetic metastable pooling electrons were separated; 3) the particle charge in the afterglow was defined by the equilibrium of electron and ion fluxes to the nanoparticle surface as in the study by Schweigert and Alexandrov [66]. The

evolution of the dust charge was simulated for a pulsed cc-rf discharge operating at p = 10 Pa (Ar/C_2H_2 mixture) and rf power modulated by a square-wave signal at frequency 0.1 kHz and 50% duty cycle. Dust particles were formed during the plasma-on phases. Denysenko et al. [99]'s simulation showed that energetic electrons generated by metastable–metastable collisions determine the charging of dust particles in the late argon plasma afterglow (a few ms in the off phase) when the dust density is high and that OML theory may not be applied for dust charging at this stage.

Kravchenko et al. [101] performed one-dimensional PIC-MCC simulations of the discharging of dust particles in the afterglow in a cc-rf discharge with planar electrodes separated by 8 cm. The argon pressure was set at p = 13.3 Pa, and the plasma was created by a sinusoidal rf voltage with 150 V amplitude and a frequency of f_{rf} = 10 MHz. The evolution of plasma parameters in the discharge gap between the two planar electrodes after switching off the rf voltage was calculated in the entire electrode gap. The simulations included secondary electron emission from dust surfaces. The simulation showed that decharging of the dust particles in the afterglow plasma occurred faster in the middle of the electrode gap because of the ion confinement at this location and because of the intense electron-ion recombination due to the collection of ions and electrons by the dust particles located in this area. Kravchenko et al. [101] also showed that the discharging rate increases with the dust particle density. Finally, their simulations showed that in the early afterglow, the plasma potential is positive relative to the electrodes, while in the later afterglow, when the electron and ion densities are significantly reduced, the amount of negative dust particles renders the "plasma" potential negative relative to the electrodes, which contributes to the effective diffusion of the dust particles toward the discharge chamber wall.

3 Modeling of temporal plasma afterglow, dust charges, and dust dynamics

When the power source of a discharge is switched off, the energy deposited in the plasma (ionization and excitation of metastable species) slowly relaxes (radiative or collisional processes) and the charge species (electrons and ions) diffuse toward the wall of the reactor [35]. For simplicity, only mono-atomic rare gases are considered here. Indeed, for such gases in the range of pressure usually used in dusty plasma experiments (1–100 Pa), plasma losses are mainly due to diffusion-recombination on surfaces (chamber wall and dust particles), and volume recombination can be neglected. In addition, assuming that ℓ is the typical spatial dimension of a laboratory discharge, the transport of charged particles can be considered diffuse and ambipolar when $\lambda_i = 1/n_g\sigma_i < \ell$, where n_g is the neutral gas number density. For argon, assuming an ion-neutral cross-section for momentum transfer $\sigma_i \sim 10^{-18}$ m^2 and ℓ ~ 10 cm, it occurs when $p \geq 1$ Pa [102,103]. Moreover, due to their lack of chemical activity, the final state of a pure rare gas afterglow is identical to its initial state before the plasma was ignited.

A good overall description of the evolution of a plasma afterglow can be obtained using the continuity equation and energy conservation. In this section, only ions and electrons are considered. The dust particles are considered fixed since the time scale for their motion is generally much larger than the afterglow timescale (the dust density n_d is, therefore, not a function of time). The plasma energy is assumed to be carried almost entirely by the electrons, as is generally the case in electrically sustained discharges [103]: the important parameter is, then, the (effective) electron temperature which relaxes toward the gas temperature in the afterglow.

The continuity equation for electrons and ions is [102,104]

$$\frac{\partial n_{i(e)}}{\partial t} + \nabla \cdot \Gamma_{i(e)} = S_{i(e)} - L_{i(e)}, \tag{1}$$

where $n_{i(e)}$ is the ion (electron) density, $\Gamma_{i(e)} = \mathrm{sgn}(q_{i(e)})n_{i(e)}\mu_{i(e)}\mathbf{E} - D_{i(e)}\nabla n_{i(e)}$ is the ion (electron) flux with $\mu_{i(e)} = e/m_{i(e)}\nu_{i(e)}$ as the ion (electron) mobility and $D_{i(e)} = k_B T_{i(e)}/m_{i(e)}\nu_{i(e)}$ as the ion (electron) diffusion coefficient. k_B is the Boltzmann constant, $T_{i(e)}$ is the ion (electron) temperature, $m_{i(e)}$ is the ion (electron) mass, and $\nu_{i(e)}$ is the ion (electron)-neutral collision frequency. $S_{i(e)}$ is the volume source term for ion (electron), and $L_{i(e)}$ is the volume loss term. In the presence of dust particles, the volume lost terms include their contribution. In the absence of externally applied electric field[1], $\mathbf{E}$ is given by the Poisson equation:

$$\nabla \cdot \mathbf{E} = -\frac{e(n_e - n_i)}{\varepsilon_0}, \tag{2}$$

where ε_0 is the vacuum permittivity. To obtain a good picture of the evolution of a plasma afterglow, it is generally sufficient to consider specially averaged global model [Lieberman and Ashida [105] and Liu et al. [40] for dust-free discharges and Denysenko et al. [65,70–73,99] and Couëdel et al. [61,82] for dusty plasma]. In that case, the balance equation for ions and electrons created in the plasma are:

$$\frac{\partial n_e}{\partial t} = K_{iz}(T_e)n_g n_e - \frac{n_e}{\tau_{We}} - K_d^e(T_e, T_i, n_e)n_e n_d, \tag{3}$$

1 The case of ambipolar diffusion in the presence of an external electric field (voltage difference between two planar electrodes, for example) is discussed by Hoyaux [113], [114]. In that case, the current collected by the negatively biased electrode will have a pure ionic component and be limited by the rate at which positive ions become available at the sheath edge, that is, by the rate at which the positive ions drift by ambipolar diffusion. The current imposed on the external field does not strongly modify the ambipolar diffusion mechanism.

$$\frac{\partial n_\mathrm{i}}{\partial t} = K_{iz}(T_\mathrm{e}) n_\mathrm{g} n_\mathrm{e} - \frac{n_\mathrm{i}}{\tau_\mathrm{We}} - K_\mathrm{d}^\mathrm{i}(T_\mathrm{e}, T_\mathrm{i}, n_\mathrm{i}) n_\mathrm{i} n_\mathrm{d}, \quad (4)$$

where $K_{iz}(T_\mathrm{e})$ is the ionization rate, τ_We and τ_Wi are the electron and ion diffusion time toward the wall of the reactor, respectively and, $K_\mathrm{d}^\mathrm{e}(T_\mathrm{e}, T_\mathrm{i}, n_\mathrm{e})$ and $K_\mathrm{d}^\mathrm{i}(T_\mathrm{e}, T_\mathrm{i}, n_\mathrm{i})$ are the electron and ion absorption rate by the dust particles, respectively. The ion (electron) absorption frequency is, thus, $\tau_{a_{\mathrm{i}(e)}}^{-1} = K_\mathrm{d}^{\mathrm{i}(e)} n_\mathrm{d}$. Other mechanisms can be included in the balance equations, such as metastable pooling and secondary emission due to ion/metastable atom collisions with the dust particles [56,65,70–72,99], but for the sake of simplicity, they are not discussed here. Note that the ionization rate, the dust absorption rate, and the diffusion time depend on the shape of the IEDF and the EEDF. In addition, the ion dust absorption rate can also depend on ion-neutral collisions [6,27]. The ion and electron dust absorption rates are linked to the time evolution of the dust particle charge number Z_d by

$$\frac{\partial Z_\mathrm{d}}{\partial t} = K_\mathrm{d}^i n_\mathrm{i} - K_\mathrm{d}^e n_\mathrm{e}. \quad (5)$$

At the beginning of the afterglow phase (or when the power source is still on), the dust particle charge number is linked to the electron, ion, and dust densities by the quasi-neutrality conditions:

$$Z_\mathrm{d} n_\mathrm{d} + n_\mathrm{i} - n_\mathrm{e} = 0. \quad (6)$$

At equilibrium, $\partial Z_\mathrm{d}/\partial t|_{Z_\mathrm{d}=Z_\mathrm{d}^\mathrm{eq}} = 0$. However, dust charging is a dynamic process, and the dust particle charge fluctuates around its equilibrium position. The typical dust charge fluctuation time scale τ_Z is linked to the plasma and dust parameters [51,84,106]. Using the OML theory [100] and assuming Maxwellian EEDF and IEDF to calculate τ_Z, one finds [27,51]

$$\frac{1}{\tau_Z} \simeq \frac{r_\mathrm{d} v_{T_\mathrm{i}}}{4\lambda_{D\mathrm{i}0}^2}\left(1 + \frac{e^2|Z_\mathrm{d}|}{r_\mathrm{d} T_\mathrm{e}}\right)\frac{n_\mathrm{i}(t)}{n_{\mathrm{i}_0}}, \quad (7)$$

where $v_{T_\mathrm{i}} = \sqrt{8k_\mathrm{B}T_\mathrm{i}/\pi m_\mathrm{i}}$ is the ion thermal velocity, n_{i_0} is the ion density in the steady-state plasma (or at the beginning of the afterglow) and $\lambda_{D\mathrm{i}0} = \sqrt{\varepsilon_0 k_\mathrm{B} T_\mathrm{i}/n_{\mathrm{i}_0} e^2}$ is the initial ion Debye length. In a typical laboratory dusty argon plasma ($n_{\mathrm{i}_0} \sim 10^9$ cm^{-3}, $T_\mathrm{e}/T_\mathrm{i} \sim 100$), Z_d^{eq} is usually negative. Using OML theory with Maxwellian ion and electron energy distribution functions $Z_\mathrm{d}^{eq} = -1675 \cdot r_\mathrm{d}(\mu\mathrm{m}) \cdot T_\mathrm{e}(\mathrm{eV})$ [27] and the characteristic time scale for dust charging is $\tau_Z \sim 1$ µs[83] (Table 1). As the plasma decays, the dust charging time increases until it exceeds the diffusion time. It should be noted that it is possible to work directly with the dust charge distribution to take into account the random character of the charging processes and, therefore, dust charge fluctuations [82,107].

In the early stage of the afterglow, if n_d is not too large so that the total charge carried by the dust particles can be neglected, electron and ion diffuse together, and the flux of ions and electrons at the wall are equal (ambipolar diffusion)[2]. In that case, the electron and ion diffusion times are equal:

$$\tau_\mathrm{We}^{-1} = \tau_\mathrm{Wi}^{-1} = \frac{u_\mathrm{B} A_\mathrm{eff}}{V}, \quad (8)$$

where $u_\mathrm{B} = \sqrt{k_\mathrm{B} T_\mathrm{e}/m_\mathrm{i}}$ is the Bohm velocity, V is the plasma volume, and A_eff is the effective area for particle loss. For a cylindrical discharge of radius R and height l, $V = \pi R^2 l$, and the effective area is [102,105,108]

$$A_\mathrm{eff} = 2\pi R^2 h_l + 2\pi R l h_R, \quad (9)$$

with [102]:

$$h_l \approx \frac{0.86}{\left[3 + l/2\lambda_i + \left(0.86 l u_\mathrm{B}/\pi D_a\right)^2\right]^{1/2}}, \quad (10)$$

$$h_R \approx \frac{0.8}{\left[4 + R/\lambda_i + \left(0.8 R u_\mathrm{B}/2.405 J_1(2.405) D_a\right)^2\right]^{1/2}}, \quad (11)$$

where J_1 is the first order Bessel function and $D_a \simeq D_\mathrm{i}(1 + T_\mathrm{e}/T_\mathrm{i})$ is the ambipolar diffusion coefficient. In the "high pressure" regime, when $\lambda_i \ll (R, l)$, the diffusion times are [102,103]

$$\tau_\mathrm{We}^{-1} = \tau_\mathrm{Wi}^{-1} \simeq D_a/\Lambda^2, \quad (12)$$

where Λ is the characteristic scale length for diffusion (in cylindrical geometry $\Lambda^{-2} = (2.405/R)^2 + (\pi/l)^2$). In argon, assuming $\Lambda \sim 1$ cm, this is the case for $p \gtrsim 1$–10 Pa [103].

TABLE 1 Afterglow time scales for an argon plasma for two pressures. A cylindrical chamber with $R = l = 4$ cm ($\Lambda = 1$ cm) is considered. The plasma parameters at the beginning of the afterglow phase are $T_\mathrm{e} = 3$ eV, $T_\mathrm{i} = T_\mathrm{gas} = 0.03$ eV, and $n_\mathrm{e} = n_\mathrm{i} = 10^9$ cm^{-3}. The electron-neutral elastic collision rate is set to $K_{el} = 10^{-13}$ m^3/s, and the ion-neutral cross-section is set to $\sigma_i = 10^{-18}$ m^2. A single particle of radius $r_\mathrm{d} = 5$ μm is considered.

	p = 10 Pa	p = 100 Pa
τ_T (μs)	10	14
τ_{coll} (μs)	175	18
τ_{wall} (μs)	11	66
$\tau_W(T_\mathrm{e} = 3$ eV) (ms)	0.04	0.25
$\tau_W(T_\mathrm{e} = 0.03$ eV) (ms)	1.2	11
$\tau_Z(T_\mathrm{e} = 3$ eV, $n_\mathrm{i} = n_0$) (μs)	0.9	0.9
$\tau_Z(T_\mathrm{e} = 0.03$ eV, $n_\mathrm{i} = n_0$) (μs)	0.6	0.6
$\tau_Z(T_\mathrm{e} = 0.03$ eV, $n_\mathrm{i} = n_0 \cdot (\lambda_{D_i^0}/\Lambda^2))$ (ms)	38	38

2 For dust density larger than 10^2 cm^{-3}, ambipolar diffusion is strongly affected by the presence of charged dust particles which can drastically reduce the electron density in the plasma [47–50]. In order to take this effect into account, considering that the total ion and electron fluxes to the walls remain equal since n_d does not change during the afterglow ($n_\mathrm{e}/\tau_\mathrm{We} = n_\mathrm{i}/\tau_\mathrm{Wi}$), it leads to a reduction of the electron diffusion time: $\tau_\mathrm{We} = \tau_\mathrm{Wi} \cdot n_\mathrm{e}/n_\mathrm{i}$ [65]. Obtaining τ_Wi when n_d is large remains an open issue.

Ambipolar diffusion relies on the fundamental property of plasmas: quasi-neutrality, that is, charge neutrality over length scales larger than the electron Debye length $\lambda_{D_e} = \sqrt{\varepsilon_0 k_B T_e / n_e e^2}$. In the afterglow, this characteristic length scale increases as the electron density decreases. When $\lambda_{D_e} \gg \Lambda$ (very low density), space charge effect become negligible and electrons and ions diffuse independently from each other. When $\lambda_{D_e} \sim \Lambda$, the diffusion is neither ambipolar nor free: it is the ambipolar-to-free diffusion transition regime. During the transition, the diffusion rate to the walls of electrons and ions toward the walls first accelerate up to the point that the ions can no longer follow. Then, the ion diffusion coefficient decreases and becomes lower than that of the electrons. The ion diffusion time $\tau_{Wi} = (D_{si}/\Lambda^2)^{-1}$ with D_{si} the ion effective diffusion coefficient becomes gradually larger than the electron diffusion time $\tau_{We} = (D_{se}/\Lambda^2)^{-1}$ with D_{se} the electron effective diffusion coefficient. It leads to the formation of a positive space charge [42–45,85,86]. Freiberg and Weaver [85] showed that the transition starts when $\Lambda/\lambda_{D_e} \sim 100$. Platier et al. [88] have recently measured that the transition starts at $\Lambda/\lambda_{De} \sim 6$, which is significantly lower than 100. The difference was explained by the influence of diffusion (evaporative) cooling of the free electrons [36–41]. An approximation of D_{se} as a function of Λ/λ_{D_e} is [109]

$$\frac{D_{se}}{D_a} = \left[\frac{1 + (\Lambda/\lambda_{D_e})^2}{(D_a/D_e) + (\Lambda/\lambda_{D_e})^2}\right]. \tag{13}$$

It is of note that Eq. 13 underestimates the real value of D_{se} [109]. Phelps [45] presents more accurate results on the effective diffusion coefficients for both ions and electrons. When the plasma contains dust particles, the dust particle charge evolution is affected by the transition from ambipolar to free diffusion [82,83]. In pulsed discharges, if the afterglow phase is shorter than the time it takes for the electron density to decrease to a value, such that $\lambda_{D_e} \gg \Lambda$, the transition from ambipolar to free diffusion can be ignored. For an argon discharge after electron thermalization ($T_e = T_i = 0.03$ eV, the thermalization process is explained below), with $n_{i_0} = n_{e_0} \sim 10^9$ cm^{-3}, p ~10–100 Pa and $\Lambda \sim 1$ cm, the transition from ambipolar to free diffusion starts after t_c ~10–100 ms. When n_d is large, the plasma losses on the dust particles can significantly diminish the plasma decay time [46,61,83]. The transition might also be affected by the presence of an external electric field and/or dust particles (especially at high dust number density), but to the best of the author's knowledge, no dedicated studies on these issues have been performed.

The evolution of the electron temperature during the afterglow needs now to be discussed. As seen above, the electron temperature is an essential parameter for both the diffusion process and the dust particle charging process. The time evolution of the electron temperature can be obtained from the power balance equation Ashida et al. [108]; Lieberman and Ashida [105]; Lieberman and Lichtenberg [102]:

$$\begin{aligned}\frac{1}{T_e}\frac{dT_e}{dt} = &-\left(\frac{2E_{iz}}{3T_e} + 1\right)K_{iz}(T_e)n_g - \frac{2E_{ex}}{3T_e}K_{ex}(T_e)n_g - 2\frac{m_e}{m_i}K_{el}(T_e)n_g \\ &-\left(\frac{2}{3}\frac{\Phi_s + \frac{5}{2}T_e}{T_e} - 1\right)\frac{u_B A_{eff}}{V} - \left(\frac{2}{3}\frac{\Phi_p + \frac{5}{2}T_e}{T_e} - 1\right)K_d^e(T_e)n_d,\end{aligned} \tag{14}$$

where $K_{ex,ell}$ are the excitation (inelastic collisions) and elastic collision rates with the neutral atom, respectively, and $\Phi_{s,p}$ are the sheath and dust surface potential, respectively. E_{iz} and E_{ex} are the ionization energy and excitation energy, respectively. In Eq. 14, energy losses due to charged particle collections by dust are supposed equivalent to the energy losses on the reactor walls. Considering that in argon $\Phi_s \simeq \Phi_p \simeq T_e \ln(\frac{m_i}{2\pi m_e})^{1/2}$ (floating potential of a flat wall, [102]), then, the terms in parenthesis in Eq. 14 have the numerical value ≈ 4 in argon [102]. Since the ionization and excitation rate fall very quickly with electron temperature, Eq. 14 can be simplified to

$$\begin{aligned}\frac{1}{T_e}\frac{dT_e}{dt} &= -\frac{2m_e}{m_i}K_{el}(T_e)n_g - 4\frac{u_B A_{eff}}{V} - 4K_d^e(T_e)n_d, \\ &= -\left(\tau_{coll}^{-1} + \tau_{wall}^{-1} + \tau_{dust}^{-1}\right) = -\tau_T^{-1}.\end{aligned} \tag{15}$$

In Eq. 15, the first term correspond the the cooling by collisions with the neutral gas background with a rate $\tau_{coll}^{-1} = 2(m_e/m_i)K_{el}(Te)n_g$. The second and third term in the right hand side of Eq. 15 correspond to the cooling of electrons by diffusion to the walls and to the dust particles with the rates $\tau_{diff}^{-1} \simeq 4u_B A_{eff}/V \simeq 4\tau_{We}^{-1}$ and $\tau_{dust}^{-1} \simeq 4K_d^e(T_e)n_d \simeq 4\tau_{a_e}^{-1}$, respectively. τ_T^{-1} is the total electron cooling rate. Diffusion cooling is important at low pressure and can even lead to electron temperature below the gas temperature and a noticeable reduction of the ambipolar diffusion coefficient below the value expected for an electron temperature equal to the gas temperature [37]. For argon, the "over-cooling" can occur for gas pressure below $p_{0_c} = 0.095$ Torr (12.7 Pa) [37]. Note that Eqs 14 and 15 are a very simplified picture of electron cooling. Indeed, Bräuer et al. [110] showed that the electron velocity distribution function is strongly modified in the first tens of microseconds of the plasma decay and is substantially influenced by collisions between metastable atoms. Godyak [111] confirmed that the EEDF is usually different in the elastic, inelastic, and electron escape (electron with energy higher than the sheath potential) energy ranges. Godyak [111] also confirmed that electron cooling is faster at low gas pressures. Liu et al. [40] showed that plasma density profile has a significant influence on the plasma density decay rate and that electron cooling rate significantly decreases with decreasing plasma density (lower e-e scattering process generating energetic electrons that can escape to the walls). Finally, Proshina et al. [41] showed that electron cooling has two different time stages: 1) rapid decrease of the electron temperature due to inelastic electron collisions with Ar atoms in the ground state, followed by 2) diffusion along the electron energy scale *via* Coulomb or elastic collisions leading to gradual electron cooling. They also

confirmed the non-Maxwellian nature of the EEDF during the electron cooling stage. All of these phenomena can have an importance for the dust charge evolution in the afterglow and are sometimes taken into account (Denysenko et al. [71–73]). Shin et al. [112] showed that in the first tens of microseconds in the afterglow, electron and positive ion densities do not decay appreciably near the plasma edge due to the transport of ions and electrons from the higher density central region of the plasma. Moreover, as can be seen from Eq. 15, the temperature decay time is always shorter than the electron and ions diffusion times. Considering constant plasma density, this allows one to estimate the temperature decay time. Taking a dust-free plasma in a cylindrical chamber with $R = l = 4$ cm ($\Lambda = 1$ cm) with $T_e = 3$ eV, $T_i = T_{gas} = 0.03$ eV, $n_e = n_i = 10^9$ cm^{-3}, $K_{el} = 10^{-13}$ m^3/s, and $\sigma_i = 10^{-18}$ m^2, one gets for an argon pressure $p = 10$ Pa $\tau_{coll} \simeq 175$ µs and $\tau_{wall} \simeq 10$ µs($\tau_T \simeq 10$ µs). Increasing the pressure to $p = 100$ Pa, one gets $\tau_{coll} \simeq 18$ μs and $\tau_{wall} \simeq 66$ µs ($\tau_T \simeq 14$ µs). As can be seen, the considered range of pressure, both the contribution of diffusion and collisions to electron cooling are important. At high dust density, the dust particles can also contribute significantly to electron cooling. The different time scales in the afterglow are summarized in Table 1. As can be seen, the electron cooling time τ_T is always of the order of a few tens of μs and, thus, in some studies, the electron cooling stage is sometimes simplified to a simple decay of the T_e with a time constant τ_T set to a few tens of μs [70].

The simulation of the time evolution of a dusty plasma afterglow requires simultaneously solving Eqs 3, 5, and 14 and evaluating the different rates as a function of the plasma parameters (and external applied field if needed) at each time step. The quasi-neutrality condition (Eq. 6) should be used to get the starting dust charge and electron density for given ion and dust densities, dust radius, initial electron temperature, and gas (ion) temperature.

4 Conclusion

In this review article, the main experimental results on temporal dusty plasma afterglow were presented.

When the power source of the discharge is turned off, the charged species of the plasma diffuse away and recombine into neutral species. When dust particles are present in the plasma, the diffusion of charged species and the plasma decay dynamics is changed. Under specific conditions, it can even lead to anomalous density increase in the early afterglow, as observed in pulsed dusty plasma discharges. Experiments have shown that large dust density can considerably shorten the plasma decay time and that metastable species and other chemically active species have an important effect in the early afterglow.

Moreover, dust particle charges also evolve during the afterglow period due to the changing plasma parameters. In the late afterglow, dust particles can keep residual charges. The value of these residual charges strongly depends on the ambipolar-to-free diffusion transition. In addition, the presence of a dc electric field, causing ions to drift through the neutral gas, has a strong influence on the final dust particle residual charges, eventually leading to large positive residual charges.

Finally, the basics of afterglow evolution modeling were presented. Dust particle contribution to plasma decay was discussed, and different electron cooling mechanisms were given.

Note that neither the discharge geometry effects nor the dust particle spatial distribution effects on the dynamics of the dusty plasma afterglow were discussed. These effects are known to be significant but are very specific to each experiment and are beyond the scope of the present review. In addition, the shape of the dust particles (only spherical particles were considered here) and the particle material can affect the charging/decharging process. Therefore, detailed studies of temporal dusty afterglow plasma are still needed. In particular, the influences of dust density and dust spatial distribution and the influences of dust shape and dust material on the diffusion of ions and electrons (including the transition from ambipolar to free diffusion) and the charging/decharging processes need to be investigated in detail. The influence of an external electric field on diffusion, especially on the transition from ambipolar to free diffusion, also requires more investigation.

Author contributions

LC performed the bibliography research necessary for the article and wrote the entire manuscript.

Funding

Natural Sciences and Engineering Research Council of Canada (NSERC), Grant No. RGPIN-2019-04333.

Acknowledgments

LC acknowledges the support of the Natural Sciences and Engineering Research Council of Canada (NSERC).

Conflict of interest

The author declares that the research was conducted in the absence of any commercial or financial relationships that could be construed as a potential conflict of interest.

Publisher's note

All claims expressed in this article are solely those of the authors and do not necessarily represent those of their affiliated organizations, or those of the publisher, the editors, and the reviewers. Any product that may be evaluated in this article, or claim that may be made by its manufacturer, is not guaranteed or endorsed by the publisher.

References

1. Bouchoule A. *Dusty plasmas: Physics, chemistry and technological impacts in plasma processing*. New York: John Wiley & Sons (1999).

2. Shukla PK, Mamun AA. *Introduction to dusty plasma*. Bristol: IOP Publishing (2002).

3. Morfill GE, Tsytovich VN, Thomas H. Complex plasmas: Ii. elementary processes in complex plasmas. *Plasma Phys Rep* (2003) 29:1–30. doi:10.1134/1.1538499

4. Fortov V, Ivlev A, Khrapak S, Khrapak A, Morfill G. Complex (dusty) plasmas: Current status, open issues, perspectives. *Phys Rep* (2005) 421:1–103. doi:10.1016/j.physrep.2005.08.007

5. Morfill GE, Ivlev AV. Complex plasmas: An interdisciplinary research field. *Rev Mod Phys* (2009) 81:1353–404. doi:10.1103/RevModPhys.81.1353

6. Melzer A. *Physics of dusty plasmas*. Berlin, Germany: Springer-Verlag GmbH (2019).

7. Fortov V, Nefedov A, Vaulina O, Lipaev A, Molotkov V, Samaryan A, et al. Dusty plasma induced by solar radiation under microgravitational conditions: An experiment on board the mir orbiting space station. *J Exp Theor Phys* (1998) 87:1087–97. doi:10.1134/1.558598

8. Samarian AA, Vaulina OS. Uv-induced coulomb structure in discharge plasma. *Phys Lett A* (2000) 278:146–51. doi:10.1016/s0375-9601(00)00730-1

9. Wang X, Horányi M, Robertson S. Experiments on dust transport in plasma to investigate the origin of the lunar horizon glow. *J Geophys Res* (2009) 114:n/a. doi:10.1029/2008JA013983

10. Smirnov RD, Pigarov AY, Rosenberg M, Krasheninnikov SI, Mendis DA. Modelling of dynamics and transport of carbon dust particles in tokamaks. *Plasma Phys Control Fusion* (2007) 49:347–71. doi:10.1088/0741-3335/49/4/001

11. Vignitchouk L, Delzanno GL, Tolias P, Ratynskaia S. Electron reflection effects on particle and heat fluxes to positively charged dust subject to strong electron emission. *Phys Plasmas* (2018) 25:063702. doi:10.1063/1.5026384

12. Autricque A, Khrapak SA, Couëdel L, Fedorczak N, Arnas C, Layet J-M, et al. Electron collection and thermionic emission from a spherical dust grain in the space-charge limited regime. *Phys Plasmas* (2018) 25:063701. doi:10.1063/1.5032153

13. Nefedov AP, Morfill GE, Fortov VE, Thomas HM, Rothermel H, Hagl T, et al. Pke-nefedov: Plasma crystal experiments on the international space station. *New J Phys* (2003) 5:33. doi:10.1088/1367-2630/5/1/333

14. Thomas HM, Morfill GE, Fortov VE, Ivlev AV, Molotkov VI, Lipaev AM, et al. Complex plasma laboratory pk-3 plus on the international space station. *New J Phys* (2008) 10:033036. doi:10.1088/1367-2630/10/3/033036

15. Pustylnik MY, Fink MA, Nosenko V, Antonova T, Hagl T, Thomas HM, et al. Plasmakristall-4: New complex (dusty) plasma laboratory on board the international space station. *Rev Sci Instrum* (2016) 87:093505. doi:10.1063/1.4962696

16. Rothermel H, Hagl T, Morfill GE, Thoma MH, Thomas H. Gravity compensation in complex plasmas by application of a temperature gradient. *Phys Rev Lett* (2002) 89:175001. doi:10.1103/PhysRevLett.89.175001

17. Schwabe M, Rubin-Zuzic M, Zhdanov S, Thomas HM, Morfill GE. Highly resolved self-excited density waves in a complex plasma. *Phys Rev Lett* (2007) 99:095002. doi:10.1103/PhysRevLett.99.095002

18. Watanabe Y. Formation and behaviour of nano/micro-particles in low pressure plasmas. *J Phys D Appl Phys* (2006) 39:R329–61. doi:10.1088/0022-3727/39/19/R01

19. Cavarroc M, Mikikian M, Tessier Y, Boufendi L. Instabilities during the growth of dust successive generations in silane-based plasmas. *Phys Plasmas* (2008) 15:103704. doi:10.1063/1.2998835

20. Qin Y, Kortshagen UR, Aydil ES. Laser light scattering from silicon particles generated in an argon diluted silane plasma. *J Phys D Appl Phys* (2016) 49:085203. doi:10.1088/0022-3727/49/8/085203

21. Groth S, Greiner F, Tadsen B, Piel A. Kinetic mie ellipsometry to determine the time-resolved particle growth in nanodusty plasmas. *J Phys D Appl Phys* (2015) 48:465203. doi:10.1088/0022-3727/48/46/465203

22. Mitic S, Coussan S, Martin C, Couëdel L. Hydro-carbon material design in a capacitively coupled radio-frequency discharge. *Plasma Process Polym* (2018) 15:1700152. doi:10.1002/ppap.201700152

23. Couëdel L, Artis D, Khanal MP, Pardanaud C, Coussan S, LeBlanc S, et al. Influence of magnetic field strength on nanoparticle growth in a capacitively-coupled radio-frequency ar/c2h2 discharge. *Plasma Res Express* (2019) 1:015012. doi:10.1088/2516-1067/ab045e

24. Samsonov D, Goree J. Particle growth in a sputtering discharge. *J Vacuum Sci Technol A: Vacuum Surf Films* (1999) 17:2835–40. doi:10.1116/1.581951

25. Mikikian M, Boufendi L. Experimental investigations of void dynamics in a dusty discharge. *Phys Plasmas* (2004) 11:3733–7. doi:10.1063/1.1761578

26. Arnas C, Chami A, Couëdel L, Acsente T, Cabié M, Neisius T. Thermal balance of tungsten monocrystalline nanoparticles in high pressure magnetron discharges. *Phys Plasmas* (2019) 26:053706. doi:10.1063/1.5095932

27. Piel A. Plasma crystals: Experiments and simulation. *Plasma Phys Control Fusion* (2017) 59:014001. doi:10.1088/0741-3335/59/1/014001

28. Couëdel L, Nosenko V. Stability of two-dimensional complex plasma monolayers in asymmetric capacitively-coupled radio-frequency discharges. *Phys Rev E* (2022) 105:015210. doi:10.1103/PhysRevE.105.015210

29. Khrapak S, Morfill G. Basic processes in complex (dusty) plasmas: Charging, interactions, and ion drag force. *Contrib Plasma Phys* (2009) 49:148–68. doi:10.1002/ctpp.200910018

30. Hutchinson IH. Forces on a small grain in the nonlinear plasma wake of another. *Phys Rev Lett* (2011) 107:095001. doi:10.1103/PhysRevLett.107.095001

31. Khrapak SA, Ivlev AV, Morfill GE. Shielding of a test charge: Role of plasma production and loss balance. *Phys Plasmas* (2010) 17:042107. doi:10.1063/1.3377786

32. Nosenko V, Ivlev AV, Zhdanov SK, Fink M, Morfill GE. Rotating electric fields in complex (dusty) plasmas. *Phys Plasmas* (2009) 16:083708. doi:10.1063/1.3194272

33. Annaratone BM, Elskens Y, Arnas C, Antonova T, Thomas HM, Morfill GE. Agglomeration of mesoscopic particles in plasma. *New J Phys* (2009) 11:103013. doi:10.1088/1367-2630/11/10/103013

34. Dap S, Lacroix D, Patisson F, Hugon R, de Poucques L, Bougdira J. Agglomeration processes in carbonaceous dusty plasmas, experiments and numerical simulations. *New J Phys* (2010) 12:093014. doi:10.1088/1367-2630/12/9/093014

35. Delpech JF, Boulmer J, Stevefelt J. *Low-temperature rare-gas stationary afterglows*. Amsterdam, Netherlands: Elsevier (1976). p. 121–81. doi:10.1016/S0065-2539(08)61215-9

36. Biondi MA. Diffusion cooling of electrons in ionized gases. *Phys Rev* (1954) 93:1136–40. doi:10.1103/PhysRev.93.1136

37. Smith D, Dean AG, Adams NG. Diffusion cooling in neon, argon, and krypton afterglow plasmas. *Z Physik* (1972) 253:191–9. doi:10.1007/BF02033319

38. Trunec D, Španěl P, Smith D. Electron temperature relaxation in afterglow plasmas: Diffusion cooling. *Contrib Plasma Phys* (1994) 34:69–79. doi:10.1002/ctpp.2150340109

39. Maresca A, Orlov K, Kortshagen U. Experimental study of diffusive cooling of electrons in a pulsed inductively coupled plasma. *Phys Rev E* (2002) 65:056405. doi:10.1103/PhysRevE.65.056405

40. Liu F-X, Guo X-M, Pu Y-K. Electron cooling and plasma density decay in early afterglow of low pressure argon plasmas. *Plasma Sourc Sci Technol* (2015) 24:034013. doi:10.1088/0963-0252/24/3/034013

41. Proshina OV, Rakhimova TV, Kovalev AS, Vasilieva AN, Zotovich AI, Zyryanov SM, et al. Experimental and PIC MCC study of electron cooling—Re-heating and plasma density decay in low pressure rf ccp

argon afterglow. *Plasma Sourc Sci Technol* (2020) 29:015015. doi:10.1088/1361-6595/ab5adb

42. Allis WP, Rose DJ. The transition from free to ambipolar diffusion. *Phys Rev* (1954) 93:84. doi:10.1103/PhysRev.93.84

43. Gusinow MA, Gerber RA. Space-charge-controlled diffusion in an afterglow. *Phys Rev A (Coll Park)* (1972) 5:1802–6. doi:10.1103/PhysRevA.5.1802

44. Gerber RA, Gerardo JB. Ambipolar-to-free diffusion: The temporal behavior of the electrons and ions. *Phys Rev A (Coll Park)* (1973) 7:781–90. doi:10.1103/PhysRevA.7.781

45. Phelps A. The diffusion of charged particles in collisional plasmas: Free and ambipolar diffusion at low and moderate pressures. *J Res Natl Inst Stand Technol* (1990) 95:407. doi:10.6028/jres.095.035

46. Dimoff K, Smy PR. Dust induced quenching of an afterglow plasma. *Phys Lett A* (1970) 32:13–4. doi:10.1016/0375-9601(70)90056-3

47. Amiranashvili S, Yu MY. Ambipolar diffusion in a dusty plasma. *Phys Plasmas* (2002) 9:4825–8. doi:10.1063/1.1517049

48. Ma JX, Yu MY, Liang XP, Zheng J, Liu WD, Yu CX. Ambipolar diffusion in an inhomogeneous dusty plasma. *Phys Plasmas* (2002) 9:1584–8. doi:10.1063/1.1468234

49. Losseva TV, Popel SI, Yu MY, Ma JX. Ambipolar diffusion in complex plasma. *Phys Rev E* (2007) 75:046403. doi:10.1103/PhysRevE.75.046403

50. Losseva TV, Popel SI. Ambipolar diffusion in a complex (dusty) plasma. *Phys Scr* (2008) T131:014045. doi:10.1088/0031-8949/2008/T131/014045

51. Ivlev A, Kretschmer M, Zuzic M, Morfill GE, Rothermel H, Thomas H, et al. Decharging of complex plasmas: First kinetic observations. *Phys Rev Lett* (2003) 90:055003. doi:10.1103/PhysRevLett.90.055003

52. Berndt J, Kovacevic E, Selenin V, Stefanovic I, Winter J. Anomalous behaviour of the electron density in a pulsed complex plasma. *Plasma Sourc Sci Technol* (2006) 15:18–22. doi:10.1088/0963-0252/15/1/003

53. Winter J, Berndt J, Hong SH, Kovačević E, Stefanović I, Stepanović O. Dust formation in ar/ch4 and ar/c2h2 plasmas. *Plasma Sourc Sci Technol* (2009) 18:034010. doi:10.1088/0963-0252/18/3/034010

54. van Minderhout B, Peijnenburg T, Blom P, Vogels JM, Kroesen GMW, Beckers J. The charge of micro-particles in a low pressure spatial plasma afterglow. *J Phys D Appl Phys* (2019) 52:32LT03. doi:10.1088/1361-6463/ab2525

55. van Minderhout B, van Huijstee JCA, Platier B, Peijnenburg T, Blom P, Kroesen GMW, et al. Charge control of micro-particles in a shielded plasma afterglow. *Plasma Sourc Sci Technol* (2020) 29:065005. doi:10.1088/1361-6595/ab8e4f

56. van Minderhout B, van Huijstee JCA, Rompelberg RMH, Post A, Peijnenburg ATA, Blom P, et al. Charge of clustered microparticles measured in spatial plasma afterglows follows the smallest enclosing sphere model. *Nat Commun* (2021) 12:4692. doi:10.1038/s41467-021-23604-z

57. Sharma G, Abuyazid N, Dhawan S, Kshirsagar S, Sankaran RM, Biswas P. Characterization of particle charging in low-temperature, atmospheric-pressure, flow-through plasmas. *J Phys D Appl Phys* (2020) 53:245204. doi:10.1088/1361-6463/ab7c97

58. Suresh V, Li L, Felipe JRG, Gopalakrishnan R. Modeling nanoparticle charge distribution in the afterglow of non-thermal plasmas and comparison with measurements. *J Phys D Appl Phys* (2021) 54:275205. doi:10.1088/1361-6463/abf70c

59. Husmann E, Thimsen E, Chen X. Particle charge distributions in the effluent of a flow-through atmospheric pressure low temperature plasma. *Plasma Sourc Sci Technol* (2021) 30:075030. doi:10.1088/1361-6595/ac12c1

60. van Huijstee JCA, Blom P, Peijnenburg ATA, Beckers J. Spatio-temporal plasma afterglow induces additional neutral drag force on microparticles. *Front Phys* (2022) 10. doi:10.3389/fphy.2022.926160

61. Couëdel L, Samarian A, Mikikian M, Boufendi L. Dust density effect on complex plasma decay. *Phys Lett A* (2008) 372:5336–9. doi:10.1016/j.physleta.2008.06.047

62. Stefanovic I, Berndt J, Maric D, Samara V, Radmilovic-Radjenovic M, Petrovic ZL, et al. Secondary electron emission of carbonaceous dust particles. *Phys Rev E* (2006) 74:026406. doi:10.1103/PhysRevE.74.026406

63. Brockhaus A, Leu GF, Selenin V, Tarnev K, Engemann J. Electron release in the afterglow of a pulsed inductively-coupled radiofrequency oxygen plasma. *Plasma Sourc Sci Technol* (2006) 15:171–7. doi:10.1088/0963-0252/15/2/001

64. Stefanović I, Sadeghi N, Winter J. The influence of c 2 h 2 and dust formation on the time dependence of metastable argon density in pulsed plasmas. *J Phys D Appl Phys* (2010) 43:152003. doi:10.1088/0022-3727/43/15/152003

65. Denysenko I, Stefanović I, Sikimić B, Winter J, Azarenkov NA, Sadeghi N. A global model for the afterglow of pure argon and of argon with negatively charged dust particles. *J Phys D Appl Phys* (2011) 44:205204. doi:10.1088/0022-3727/44/20/205204

66. Schweigert IV, Alexandrov AL. Effect of nanoparticles on an rf discharge afterglow. *J Phys D Appl Phys* (2012) 45:325201. doi:10.1088/0022-3727/45/32/325201

67. Alexandrov AL, Schweigert IV, Ariskin DA. Kinetic simulations of argon dusty plasma afterglow including metastable atom kinetics. *J Exp Theor Phys* (2013) 116:663–72. doi:10.1134/S1063776113030151

68. Sikimić B, Stefanović I, Denysenko IB, Winter J. A non-invasive technique to determine ion fluxes and ion densities in reactive and non-reactive pulsed plasmas. *Plasma Sourc Sci Technol* (2013) 22:045009. doi:10.1088/0963-0252/22/4/045009

69. Sikimić B, Stefanović I, Denysenko IB, Winter J, Sadeghi N. Dynamics of pulsed reactive RF discharges in response to thin film deposition. *Plasma Sourc Sci Technol* (2014) 23:025010. doi:10.1088/0963-0252/23/2/025010

70. Denysenko IB, Stefanović I, Azarenkov NA, Burmaka GP. Effect of secondary emission on the argon plasma afterglow with large dust density. *Phys Plasmas* (2015) 22:023702. doi:10.1063/1.4907225

71. Denysenko IB, Azarenkov NA, Ostrikov K, Yu MY. Electron energy probability function in the temporal afterglow of a dusty plasma. *Phys Plasmas* (2018) 25:013703. doi:10.1063/1.5010742

72. Denysenko IB, von Wahl E, Labidi S, Mikikian M, Kersten H, Gibert T, et al. Modeling of argon–acetylene dusty plasma. *Plasma Phys Control Fusion* (2019) 61:014014. doi:10.1088/1361-6587/aade2d

73. Denysenko IB, Stefanović I, Mikikian M, Kovacevic E, Berndt J. Argon/dust and pure argon pulsed plasmas explored using a spatially-averaged model. *J Phys D Appl Phys* (2021) 54:065202. doi:10.1088/1361-6463/abc210

74. Barkan A, Merlino RL. Confinement of dust particles in a double layer. *Phys Plasmas* (1995) 2:3261–5. doi:10.1063/1.871159

75. Saxena V, Avinash K, Sen A. Dust cluster explosion. *Phys Plasmas* (2012) 19:093706. doi:10.1063/1.4754010

76. Piel A, Goree JA. Collisional and collisionless expansion of yukawa balls. *Phys Rev E* (2013) 88:063103. doi:10.1103/PhysRevE.88.063103

77. Childs MA, Gallagher A. Plasma charge-density ratios in a dusty plasma. *J Appl Phys* (2000) 87:1086–90. doi:10.1063/1.371983

78. Childs MA, Gallagher A. Small particle growth in silane radio-frequency discharges. *J Appl Phys* (2000) 87:1076–85. doi:10.1063/1.371982

79. Couëdel L, Mikikian M, Boufendi L, Samarian AA. Residual dust charges in discharge afterglow. *Phys Rev E* (2006) 74:026403. doi:10.1103/PhysRevE.74.026403

80. Mikikian M, Cavarroc M, Couëdel L, Boufendi L. Low frequency instabilities during dust particle growth in a radio-frequency plasma. *Phys Plasmas* (2006) 13:092103. doi:10.1063/1.2337793

81. Couëdel L, Samarian AA, Mikikian M, Boufendi L. Dust charge distribution in complex plasma afterglow. *Europhys Lett* (2008) 84:35002. doi:10.1209/0295-5075/84/35002

82. Couëdel L, Samarian A, Mikikian M, Boufendi L. Influence of the ambipolar-to-free diffusion transition on dust particle charge in a complex plasma afterglow. *Phys Plasmas* (2008) 15:063705. doi:10.1063/1.2938387

83. Couëdel L, Mezeghrane A, Samarian A, Mikikian M, Tessier Y, Cavarroc M, et al. Complex plasma afterglow. *Contrib Plasma Phys* (2009) 49:235–59. doi:10.1002/ctpp.200910025

84. Cui C, Goree J. Fluctuations of the charge on a dust grain in a plasma. *IEEE Trans Plasma Sci* (1994) 22:151–8. doi:10.1109/27.279018

85. Freiberg RJ, Weaver LA. Microwave investigation of the transition from ambipolar to free diffusion in afterglow plasmas. *Phys Rev* (1968) 170:336–41. doi:10.1103/PhysRev.170.336

86. Gerber RA, Gusinow MA, Gerardo JB. Transition from ambipolar to free diffusion of ions. *Phys Rev A (Coll Park)* (1971) 3:1703–7. doi:10.1103/PhysRevA.3.1703

87. Dote T, Shimada M. Transition from free to ambipolar diffusion of positive ions. *J Phys D Appl Phys* (1988) 21:210–2. doi:10.1088/0022-3727/21/1/031

88. Platier B, Limpens R, Lassise AC, Staps TJA, van Ninhuijs MAW, Daamen KA, et al. Transition from ambipolar to free diffusion in an EUV-induced argon plasma. *Appl Phys Lett* (2020) 116:103703. doi:10.1063/1.5142290

89. Wörner L, Ivlev AV, Couëdel L, Huber P, Schwabe M, Hagl T, et al. The effect of a direct current field on the microparticle charge in the plasma afterglow. *Phys Plasmas* (2013) 20:123702. doi:10.1063/1.4843855

90. Filatova I, Trukhachev F, Chubrik N. Study of the process of dust grain discharging in the afterglow of an rf discharge. *Plasma Phys Rep* (2011) 37:1042–5. doi:10.1134/S1063780X1111002X

91. Schneider V. *Optisch gefangene Mikropartikel als Sonden in einem Hochfrequenz-Niederdruckplasma*. Ph.D. thesis. Kiel, Germany: Christian-Albrechts-Universität zu Kiel (2020).

92. Chaubey N, Goree J, Lanham SJ, Kushner MJ. Positive charging of grains in an afterglow plasma is enhanced by ions drifting in an electric field. *Phys Plasmas* (2021) 28:103702. doi:10.1063/5.0069141

93. Chaubey N, Goree J. Preservation of a dust crystal as it falls in an afterglow plasma. *Front Phys* (2022) 10. doi:10.3389/fphy.2022.879092

94. Couëdel L, Samarian A, Mikikian M, Boufendi L. Dust-cloud dynamics in a complex plasma afterglow. *IEEE Trans Plasma Sci IEEE Nucl Plasma Sci Soc* (2008) 36:1014–5. doi:10.1109/TPS.2008.920220

95. Meyer JK, Merlino RL. Evolution of dust clouds in afterglow plasmas. *IEEE Trans Plasma Sci IEEE Nucl Plasma Sci Soc* (2016) 44:473–8. doi:10.1109/TPS.2015.2504920

96. Merlino RL, Meyer JK, Barkan A, Avinash K, Sen A. Coulomb explosion and fission of charged dust clusters. *AIP Conf Proc* (2018) 1925:020021. doi:10.1063/1.5020409

97. Merlino RL, Meyer JK, Avinash K, Sen A. Coulomb fission of a dusty plasma. *Phys Plasmas* (2016) 23:064506. doi:10.1063/1.4954906

98. Chaudhuri M, Couëdel L, Thomas E, Huber P, Lipaev AM, Thomas HM, et al. *Spontaneous dust pulse formation in the afterglow of complex plasmas under microgravity conditions* (2021). *arXiv:2103.09607*. doi:10.48550/ARXIV.2103.09607

99. Denysenko IB, Stefanović I, Sikimić B, Winter J, Azarenkov NA. Discharging of dust particles in the afterglow of plasma with large dust density. *Phys Rev E* (2013) 88:023104. doi:10.1103/PhysRevE.88.023104

100. Allen JE, Annaratone BM, de Angelis U. On the orbital motion limited theory for a small body at floating potential in a Maxwellian plasma. *J Plasma Phys* (2000) 63:299–309. doi:10.1017/S0022377800008345

101. Kravchenko OY, Maruschak I, Yushchyshena YV. Influence of dust particles on rf-discharge plasma afterglow. *Probl At Sci Technol* (2015) 1:220–3.

102. Lieberman MA, Lichtenberg AJ. *Principles of plasma discharges and materials processing*. Hoboken, NJ, USA: John Wiley & Sons (2005). doi:10.1002/0471724254

103. Chabert P, Braithwaite N. *Physics of radio-frequency plasmas*. Cambridge: Cambridge University Press (2011).

104. Raizer YP. *Gas discharge Physics*. Berlin: Springer (1991).

105. Lieberman MA, Ashida S. Global models of pulse-power-modulated high-density, low-pressure discharges. *Plasma Sourc Sci Technol* (1996) 5:145–58. doi:10.1088/0963-0252/5/2/006

106. Maiorov SA, Vladimirov SV, Cramer NF. Calculation of the grain charge fluctuations in a dusty plasma. *Plasma Phys Rep* (2002) 28:946–52. doi:10.1134/1.1520288

107. Mishra SK, Misra S, Sodha MS. Charge distribution over dust particles in a flowing plasma. *Phys Plasmas* (2011) 18:103708. doi:10.1063/1.3650708

108. Ashida S, Lee C, Lieberman MA. Spatially averaged (global) model of time modulated high density argon plasmas. *J Vacuum Sci Technol A: Vacuum Surf Films* (1995) 13:2498–507. doi:10.1116/1.579494

109. Moisan M, Pelletier J. *Physics of collisional plasmas*. Berlin, Germany: Springer Netherlands (2012). doi:10.1007/978-94-007-4558-2

110. Bräuer T, Gortchakov S, Loffhagen D, Pfau S, Winkler R. The temporal decay of the diffusion-determined afterglow plasma of the positive column. *J Phys D Appl Phys* (1997) 30:3223–39. doi:10.1088/0022-3727/30/23/007

111. Godyak VA. Electron energy distribution function control in gas discharge plasmas. *Phys Plasmas* (2013) 20:101611. doi:10.1063/1.4823075

112. Shin H, Zhu W, Economou DJ, Donnelly VM. Ion energy distributions, electron temperatures, and electron densities in ar, kr, and xe pulsed discharges. *J Vacuum Sci Technol A: Vacuum, Surf Films* (2012) 30:031304. doi:10.1116/1.4705515

113. Hoyaux MF. Some remarks concerning the phenomenon of ambipolar diffusion in gaseous discharges. *Am J Phys* (1967) 35:232–42. doi:10.1119/1.1974015

114. Hoyaux M. The role of ambipolar phenomena in the mechanism of the post-zero current in vacuum circuit breakers. *Proc IEEE* (1967) 55:2123–33. doi:10.1109/PROC.1967.6090